OH radical production in an atmospheric pressure surface micro-discharge array

2016 J. Phys. D: Appl. Phys. 49 455202

(http://iopscience.iop.org/0022-3727/49/45/455202)

IOP Publishing Journal of Physics D: Applied Physics

J. Phys. D: Appl. Phys. **49** (2016) 455202 (12pp) doi:10.1088/0022-3727/49/45/455202

OH radical production in an atmospheric pressure surface micro-discharge array

D Li[1,2], A Nikiforov[2,7], N Britun[3], R Snyders[3,4], M G Kong[1,5,6,7] and C Leys[2]

[1] State key Laboratory of Electrical Insulation and Power Equipment, Center for Plasma Biomedicine, Xi'an 710049, People's Republic of China
[2] Department of Applied Physics, Research Unit Plasma Technology, Ghent University, Sint-Pietersnieuwstraat 41, Ghent B-9000, Belgium
[3] Chimie des Interactions Plasma-Surface (ChIPS), CIRMAP, Université de Mons, 23, Place du Parc, B-7000 Mons, Belgium
[4] Materia Nova Research Center, Parc Initialis, B-7000 Mons, Belgium
[5] Frank Reidy Center for Bioelectrics, Old Dominion University, Norfolk, VA 23508, USA
[6] Department of Electrical and Computer Engineering, Old Dominion University, Norfolk, VA 23529, USA

E-mail: Anton.Nikiforov@UGent.be and mkong@odu.edu

Received 3 June 2016, revised 4 September 2016
Accepted for publication 9 September 2016
Published 17 October 2016

Abstract

The generation of OH radicals from an array of surface micro-discharges working in atmospheric pressure He/Ar/H_2O mixtures is investigated. The absolute OH density and its temporal-and-spatial dynamics are detected by UV broadband absorption spectroscopy (UV-BAS) and laser-induced fluorescence (LIF) spectroscopy. The measured absolute density of OH(X) state is about 10^{21} m^{-3} in Ar/H_2O mixture reaching a peak at 0.05% of H_2O. In the case of He/H_2O mixtures however, the peaking at ~10^{19} m^{-3} is approximately two orders of magnitude lower and decreases monotonously with increasing H_2O content. From a control standpoint, the ratio of the Ar/He mixture may be adjusted to tune the OH density over two orders of magnitude and to modulate the H_2O content dependence of the OH density. The capability of modulating the OH radical production over a large density range is of practical interest for many applications such as atmospheric chemistry and biochemistry. With the array of atmospheric micro-discharges sustained over a large electrode area, a uniform distribution of its OH density can be achieved in a plane parallel to the electrodes thus enabling spatially controlled surface treatment of large samples.

Keywords: surface discharge, laser-induced fluorescence, absorption spectroscopy, hydroxyl radicals

(Some figures may appear in colour only in the online journal)

1. Introduction

Atmospheric pressure non-equilibrium plasmas are widely used in many fields including biomedical applications [1, 2], liquid media treatment [3, 4] polymer modification [5] and thin film deposition [6]. Compared to low-pressure plasmas, atmospheric-pressure plasmas do not require expensive and space-limiting vacuum systems. Surface discharges belong to the class of atmospheric-pressure non-equilibrium plasmas [7, 8]. The use of a mesh electrode in surface discharge allows for controlled production of many individual micro-discharges, each in one cell of the mesh electrode thus confining plasma instability locally [9–12], and the integration of all cells within one electrode facilitates convenient up-scaling of the micro-discharges in an array for large-area applications [12]. The micro-discharges are generated on the surface of a dielectric sheet attached to the mesh electrode, and reactive species produced in the gas phase are transported to a downstream target material. Since this indirect treatment method can transfer the reactive species to a remote sample at room temperature, it

[7] Author to whom any correspondence should be addressed.

is especially suitable for treatment of heat-sensitive materials such as polymers and living tissues.

Hydroxyl radical is an important active species generated in H_2O-containing plasma, and it is considered to play an important role in applications in plasma medicine [2, 13]. Puač *et al* [14] studied bacteria inactivation by reactive species including OH radicals and it was concluded that OH radicals are more efficient in the case of treatment gram negative bacteria. Stoffels *et al* [15] found that reactive species including ground state OH(X), generated in a discharge, can provide functional manipulation of mammalian cells without cell death. By changing the lipid composition of the skin, OH is also considered to be important in a cure of the diseases like ichthyosis or atopic dermatitis [16]. Apart from being an oxidant, the OH radical is also a precursor for formation of other oxidative species, such as H_2O_2. It is therefore useful to gain a deeper insight into the generation processes of ground state OH(X) and excited state OH(A) radicals. For atmospheric-pressure surface micro-discharge arrays (SMDAs), it is particularly interesting to investigate temporal and spatial behavior related to the generation of OH radicals. The utilization of different methods for the OH radical detection provides a way to study dynamics of OH production and measurement of their absolute density. This method is used in this work to gain an insight into the physics lying behind the generation of radicals and to identify routes for optimization of OH(X) production and control.

Three methods, namely emission spectroscopy near 309 nm, absorption spectroscopy in the UV range, and laser-induced fluorescence (LIF) are often employed to study OH radicals in the literature [17]. Measurement of OH radicals has been reported for various plasma sources such as plasma jets [18–21], of which the focus is often on OH production within the plasma generation region. Fewer, if any, have been reported so far, on the OH density and its spatiotemporal distribution remote from the plasma generation region, such as in the case of atmospheric surface micro-discharge arrays (SMDAs), for which loss, transport, and reaction chemistry of the OH molecule in the exhaust region of plasma generation is important. The advantage of the UV light absorption method is related to the fact that it is independent of the collisional processes. Therefore, the interpretation of the results obtained by this method is straightforward and provides a way of cross-check the validity of LIF measurements. Wang *et al* used an adaptation of the UV absorption method, namely cavity ring-down spectroscopy (CRDS), to measure the density of OH in a microwave plasma jet [20]. The UV broadband absorption spectroscopy (UV-BAS) was applied to determine the density of OH in a radio frequency (RF) glow discharge [22] and pulsed dielectric barrier discharge (DBD) [23]. The absorption method itself is simple from an experimental point of view. A broadband UV light emitting diode (LED) source or lamp with high emission stability near 309 nm coupled with a high-resolution spectrometer are required in this case. However, the UV absorption measurements are restricted to line-of-sight detection, and so it cannot provide in-depth resolution of OH radicals, which is an important issue for micro-discharges. LIF spectroscopy is another diagnostic with high sensitivity and high temporal and space resolution, suitable for detecting the temporal-and-spatial behavior of OH density [24]. However, the collisional processes resulting in quenching of the excited states along with the vibrational energy transfer (VET) can strongly affect LIF signal and need to be taken into account in LIF measurements. By calibrating the LIF method, e.g. by means of Rayleigh scattering, the absolute density of radical can be determined. Recently, Verreycken *et al* [25] compared two methods (LIF and UV-BAS) for quantitative OH measurements in a nanosecond pulsed discharge and found a good agreement within the experimental accuracy.

In this work, UV-BAS technique, and LIF spectroscopy are applied collectively to measure the OH density and temporal-and-spatial behavior of OH(X) radicals generated by the array surface discharge. The discharge is operated in He or Ar with a varying percentage of H_2O vapour used to enhance and modulate the production of OH radicals.

2. Experimental set-up and methods

2.1. The surface micro-discharge

The SMDA used in this study was previously reported with a mesh electrode as the ground electrode [12]. The schematic diagram of the experimental set-up with different diagnostics is shown in figure 1. The high-voltage electrode consists of a solid aluminum plate of $4 \times 4\,cm^2$, a steel mesh as the ground electrode having a total area slightly larger than the aluminum plate, and a polytetrafluroethene (PTFE) plate of 1 mm thickness that is sandwiched between the two electrodes. Each mesh cell has a hexagon shape with 4 mm side length, 0.76 mm wire width and 0.5 mm mesh thickness, giving a mesh density of about 3.2 cells cm^{-2}. For plasma generation, a low-frequency 20 kHz power supply was used to provide a sinusoidal output voltage with a peak-to-peak voltage of 14 kV fixed in all experiments. A homemade 1 m long bubbler system with a micro-porous ceramic dispenser was used in order to mix H_2O vapour with the feed gas, and the gas passing through the bubbler is assumed to be saturated by H_2O vapour. Saturation of the gas flow after passing through the bubbling unit has been confirmed in our previous work [19] where the same bubbling unit has been used. In addition the water content has been measured in the same gas flow system with mass-spectroscopy method and shows the correctness of the method of H_2O estimation. The H_2O temperature in the bubbler was measured prior to every experiment with a thermometer (EXTECH, 4213015) and used to calculate the saturation H_2O pressure. Two mass flow controllers (MKS instruments controllers, model 4000) were employed to mix the flows of He, Ar or their mixture with saturated H_2O vapour. The total rate of the plasma-forming gas was fixed at 4 slm for all experiments and the basal H_2O content due to impurities in a gas bottle and air diffusion is estimated negligible low of order 0.007%. The gas inlet is located on the back side of the plasma cell that leads to rather complicated gas dynamics in the cell and non-uniform distribution of the air impurities in the discharge volume. Optical emission of the discharge

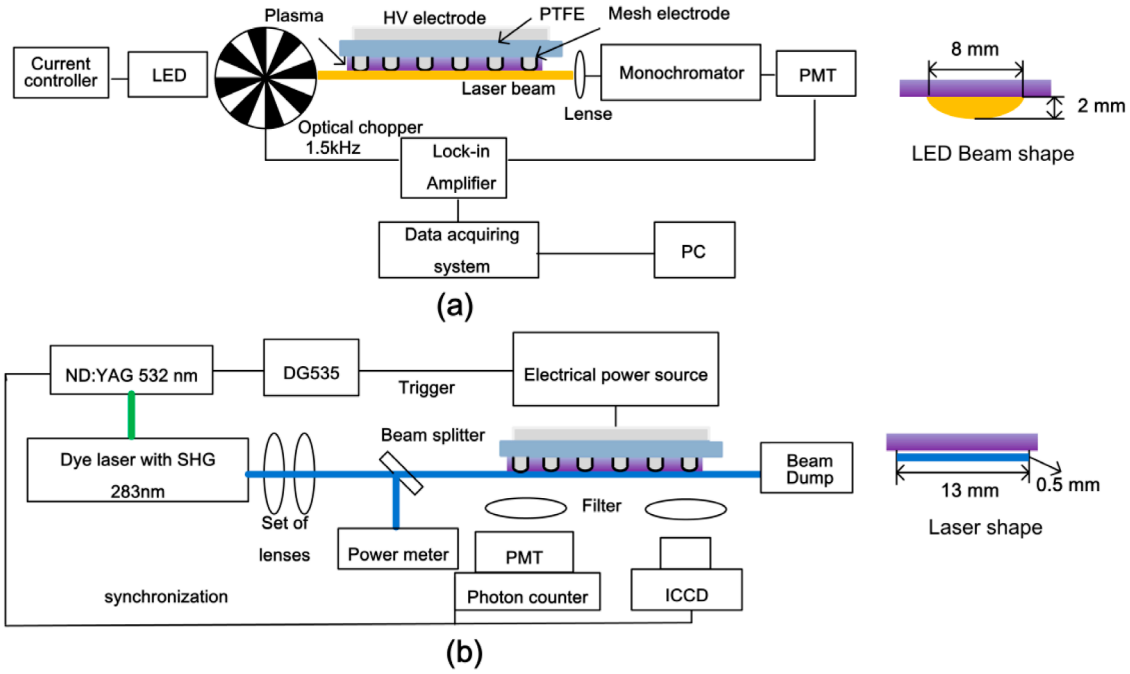

Figure 1. Experimental set-up of (a) UV broadband absorption measurement; (b) the laser diagnostics.

was acquired by an Avantes spectrometer with the resolution of 0.05 nm used to record the OH (A–X) emission bands in the range of 300–320 nm for the sake of obtaining the gas temperature (T_g) through rotational analysis. The OH (A–X) spectrum was present in discharges in pure Ar gas or in He gas due to small impurities of H_2O in the gas bottles and in the gas delivering system. The instrumental function of the spectrometer was determined using a low pressure Pen-Ray Ar lamp, and spectrometer was calibrated with the Model 63356Oriel NIST lamp (250–900 nm range).

2.2. The absorption measurements

Since optical emission spectroscopy (OES) only provides information on the excited OH(A) states, in order to investigate the generation of ground OH(X) states, two different methods were used, namely the absorption of UV radiation and LIF spectroscopy. The set-up used for UV absorption is shown in figure 1(a). The UV light emission was generated by means of a 310 nm LED light source UVTOP310 powered by the current source SRS, Model LDC501. The full width at half maximum (FWHM) of the UV light source was 10 nm. The light signal passing the plasma volume was collected with 0.75 m focal distance monochromator (Zolix, Omni-λ750) equipped with a photomultiplier tube. A lock-in amplifier (SRS, model SR850 DSP) was used for signal acquisition. The lock-in amplification technique allows for measurement of very low absorption signal, even if the background optical signal is a few orders of magnitude higher than the emission of interest. High signal-to-noise ratio of the lock-in method allows for detection of a very small variation of the signal (up to 10^{-3}) due to absorption through synchronization of the SR850 DSP unit (locking) with source light modulated frequency of 1.5 kHz. The spectral resolution of the system was estimated to be around 70 pm having a Gaussian line profile.

2.3. LIF measurements

LIF technique was used to detect the hydroxyl radicals by exciting the $X^2\Pi(v''=0)$ state to $A^2\sum^+(v'=1)$ state. The scheme of the system is shown in figure 1(b). A dye laser (Sirah Cobra Stretch with second harmonic generation (SHG) unit) using the Rhodamine 590 dye was pumped by a Nd:YAG laser at 532 nm. The laser has a repetition rate of 10 Hz and pulse duration of 5 ns. The LIF measurements were performed via the excitation of the ground OH state through the use of $P_1(4)$ transition around 283 nm. The laser beam was further expanded using a cylindrical UV lens to make 2.5 cm wide laser sheet in the plasma region. The shaped beam had an almost uniform profile in its central part, which was used for all the experiments reported here. The laser pulse energy, real-time monitored by a laser energy meter head (Ophir PE-9), was kept within the range of 0.4–0.5 mJ. The obtained LIF signal was laser energy corrected according to the expression $I_{LIF}^{corr} = I_{LIF}/E_{las}^{S}$, according to figure 2.

Low energy operation of the laser up to 0.5 mJ allows for its use in the linear region of the LIF measurement thus avoiding the effect of the LIF signal saturation. The OH fluorescence signal was collected in different experiments by an Andor Shamrock 750 spectrometer equipped either with an iStar740 intensified charge coupled device (ICCD) or with a Hamamatsu R928 photomultiplier tube with the optical band pass filter having a central wavelength of 309 nm and the full width at half area of 10 nm. The ICCD images were recorded with a gate width of 100 ns using 20 accumulations. Calibration of the LIF signal was carried out by the commonly used Rayleigh scattering technique [27], i.e. close to maximum transparency of the used optical filter based on 2D images of the Rayleigh scattering of the laser beam in the same shape as used for the planar LIF.

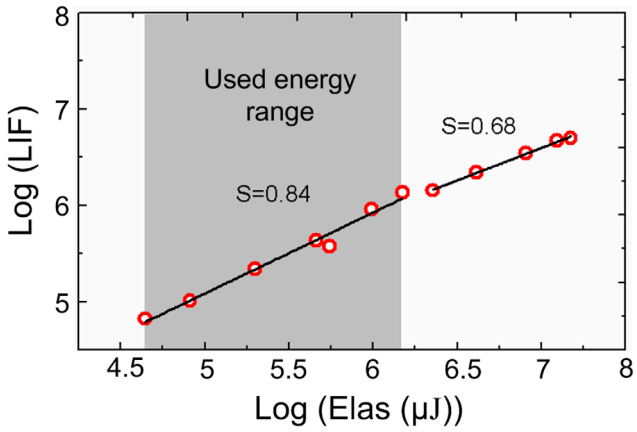

Figure 2. LIF signal intensity as a function of the measured laser energy. The non-linearity coefficient S is shown for both low and high laser energy regions. The grey area corresponds to the working energy range.

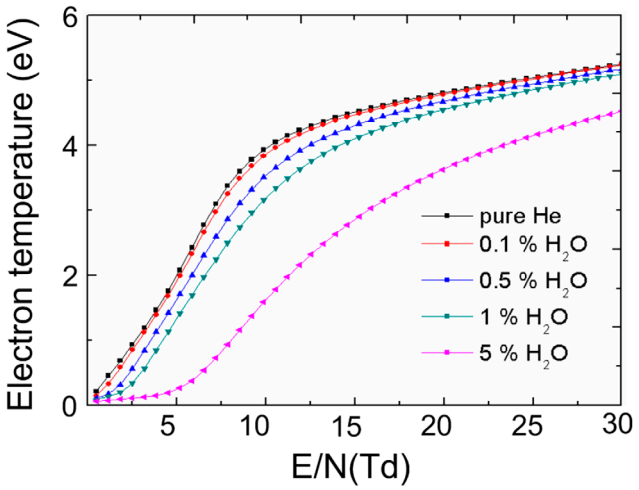

Figure 3. Effect of the H_2O admixture on the mean electron energy in the He plasma as calculated with Bolsig$^+$ [23].

3. Results and discussion

The emission spectroscopy reveals that the OH(A) emission in Ar/H_2O gas mixture is about 20 times higher than that in the He/H_2O mixture. In our opinion, the most probable explanation of the higher emission in Ar discharge is related to a difference in the discharge operation modes in Ar and He gases. In previous work [12], it was shown that SMDA is generated in glow-like mode in He gas resulting in weak but diffuse plasma uniformly distributed in the mesh cells. In contrast, discharge in Ar gas and in the mixture of H_2O is filamentary. The short filaments with a length shorter that 1 mm are formed in Ar SMDA [28] and they have higher brightness in comparison with diffuse He plasma. We expect that the T_e value can be higher locally in the filament, which leads to higher production of excited species. The decline in the OH(A) emission with increased H_2O content above 0.12% can be attributed to several processes including a decrease in the OH(X) ground state density, change to plasma properties, namely electron density n_e and electron temperature T_e, and an increase of the OH(A) state quenching by H_2O molecules. Both Ar and especially He have a relatively low collisional quenching cross-section of the OH(A) state (0.037 and 0.006 Å^2 at 400 K, respectively) whereas the quenching by H_2O is much higher (about 86 Å^2 [29]) but even so cannot explain the fast decrease of OH(A) emission.

As shown in [23], the electrons produced by the discharge can be easily attached to the H_2O molecules by impact and dissociative attachment. As a result, n_e decreases with the increase of the H_2O content, thereby leading to the drop in the generation of the excited OH(A) state [30]. However, a strong decrease of the electron density is unlikely at such a low H_2O admixture and unlikely to be responsible for the decreasing OH(A). On the other hand, the addition of H_2O into either Ar or He plasma can strongly affect the electron energy distribution function and so the electron temperature can strongly decrease even at a low admixture of the H_2O vapor. Figure 3 shows the effect of increasing of the H_2O admixture to the mean electron energy in a He discharge for a reduced electrical field of 0.5–40 Td. In the typical condition of SMDA plasmas, the expected reduced electrical field is about 15–25 Td. Data in figure 3 is calculated by solving the Boltzmann equation using the Bolsig$^+$ software [31] with 51 electron impact cross-sections of He and 10 cross-sections of H_2O from the relevant databases [32]. The results clearly indicate the importance of the effect of H_2O on T_e in noble gas discharges especially at high H_2O content above 1% but even at low H_2O admixing there is a considerable effect of H_2O on T_e and therefore on the production of OH(A) states. It has to be emphasizing here, that results presented in figure 3 are obtained considering only electron impact reactions. Clearly, 3-body collisions and reactions of neutrals and excited states with H_2O molecules can also be very important in the generation of OH states. The mechanism of OH production can be studied through the construction of a detailed collision-radiative model of the discharge which is complicated and out of the scope of this work but still such processes can be as important in OH(A) generation as the electron impact reactions.

The observed higher emission of OH(A) in the Ar mixture and the effect of H_2O admixing on emission spectroscopy results are important it terms of possible monitoring of the discharge behavior. Within the vision of the importance of the ground state OH(X) radical, a focus in this work is to put on the temporal-and-spatial dynamics of the OH(X) generation through the use of a planar LIF method and UV-BAS.

3.1. Planar LIF measurement of OH(X) radicals

The time-resolved LIF images were recorded at 309 nm using a planar laser beam passing through the discharge cell. The applied voltage was synchronized with the laser in order to obtain the time-resolved dynamics of OH(X) radicals' generation with a resolution of better than 100 ns. In addition the time-resolved images of OH(A) emission (discharge images with a band pass filter at 310 nm, FWHM of 10 nm) were recorded with the same ICCD camera.

The surface barrier discharge was generated in the air sealed box, but it is still possible that a certain amount of air impurities may be present in the plasma volume. It is well

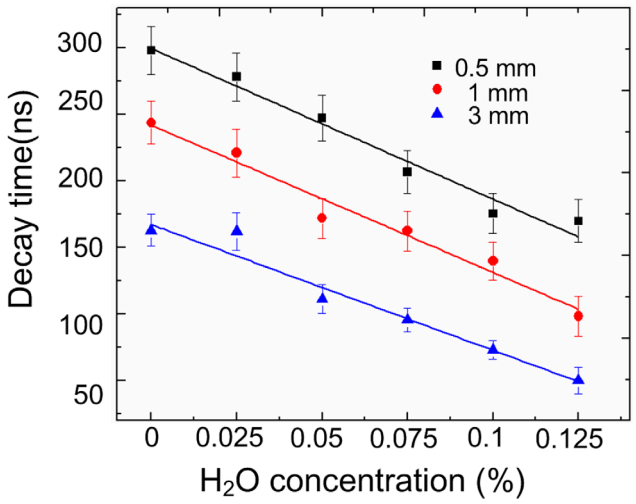

Figure 4. The decay as a function of the distance from the electrode and H_2O concentration in Ar gas. (LIF signal obtained by SR430 photon counter unit with 5 ns resolution after excitation of $P_1(4)$ transition.)

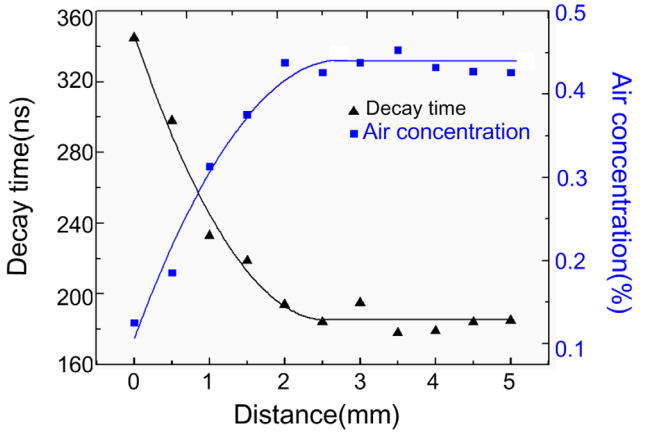

Figure 5. The LIF decay time in Ar discharge and estimated concentration of air impurity with increasing the distance from the mesh electrode.

known that both N_2 and O_2 are good quenchers of OH(A) states with rate constants at room temperatures of 13.6×10^{-11} cm^3 s^{-1} and 2.47×10^{-11} cm^3 s^{-1} [33], respectively. Also impurities of N_2 and O_2 can affect vibrational and rotational energy transfer (RET) of He excited states, and it leads to misinterpretation of the LIF results, see e.g. works [18, 19, 21] and references herein. In addition, the air impurity may help to produce some other active species to the downstream of the discharge. Accordingly, analysis of LIF images requires the knowledge of air admixing in the feed gas and air distribution in the system. The amount of air in the system has been estimated based on the measured decay of the LIF signal presented in figure 4.

The radiative decay time of excited OH(A) radicals without quenching is estimated to be about 780–1500 ns depending on the transition [34], but the LIF signal decay is much faster in the presence of effective quenchers O_2, N_2 and H_2O. The measured LIF decay time in Ar/H_2O mixture in three different positions is presented in figure 4. The decay time decreases from about 300 to 170 ns with increasing H_2O concentration to 0.12% in front of the electrode, see figure 4. Indeed, the H_2O vapor rapidly quenches the OH(A) and it shortens the decay time. However, the decay time decreases when the distance from the laser to the grounded electrode increases. This is explained by the different concentration of air impurity in the discharge volume. The shorter decay time observed is associated with additional quenching of OH(A) by N_2 and O_2 and is used to calculate the mole fraction of the air. The LASKIN software [35] was used to simulate the kinetics of the population and depopulation of the OH(A) states, and total decay of the LIF signal has been analyzed in detail in our previous work [21]. At atmospheric pressure, collisional quenching, VET and RET are important and have to be taken into account in the simulation of the decay time. The impurity of air with a different distance from the electrode, obtained by comparing experimental results and simulation, is shown in figure 5 for the Ar plasma. Similar air impurity is found in the He discharge.

It is shown in figure 5 that the air concentration increases from 0.1% in a vicinity of the electrode and reaches its peak value at $z = 2.5$ mm from the ground electrode, after that it saturates at 0.45%. The level of air impurities was constant along the electrode mesh and so LIF images can be directly related to the density of OH(X). In addition to LIF images, spatial resolved patterns of the emission of OH(A) species were collected. Time-resolved LIF and emission images at the electrode surface ($z = 0$ mm) for the discharges in He/0.02%H_2O and Ar/0.02%H_2O mixtures are presented in figures 6 and 7, respectively. In the case of He/0.02%H_2O, two broad current peaks of about 18 mA are observed in figure 6 at an interval of $t = 36$ μs to $t = 44$ μs relative to the ICCD trigger point (marked as time 0 in figure 6). In the Ar/0.02%H_2O discharge, two distinguished periods where OH(A) emission is detected are at 15 and 35 μs. The formation of the OH(A) states is not temporally uniform in a discharge cycle and it follows the waveform of applied voltage.

The obtained LIF imaging data show that the ground-state OH exists in the full cycle and the LIF intensity maintains approximately at the same level regardless of the magnitude of the applied voltage. Therefore, the OH(X) life-time exceeds 20 μs in our conditions, while its density is temporally uniform, even between the discharge pulses. The main loss mechanisms of OH(X) radicals can be found in table 1. Based on data in table 1 and results of absolute OH(X) measurements, presented below, the life-time of OH(X) at $T_g = 298$ K can be estimated as 0.42 ms for Ar/0.02% H_2O and 9.5 ms for He/0.02%H_2O. Careful analysis of the LIF patterns indicates that the OH(X) radicals are simultaneously produced in each hexagonal cell having the maximum density inside the cell. This was confirmed by the shift of the discharge in horizontal position against the laser beam. The OH(X) radicals can diffuse along z direction away from the mesh electrode to a downstream distance of 5 mm. At the distances beyond 5 mm from the ground electrode, OH(X) fluorescence is negligible in both the He/H_2O and Ar/H_2O discharges.

The measured LIF signal has been calibrated by the Rayleigh scattering of the laser beam in order to obtain absolute density of OH radicals. The simplified 4-level LIF model [25] similar to our three-level model [19, 21, 35] is used to describe kinetics of the excited and the ground state

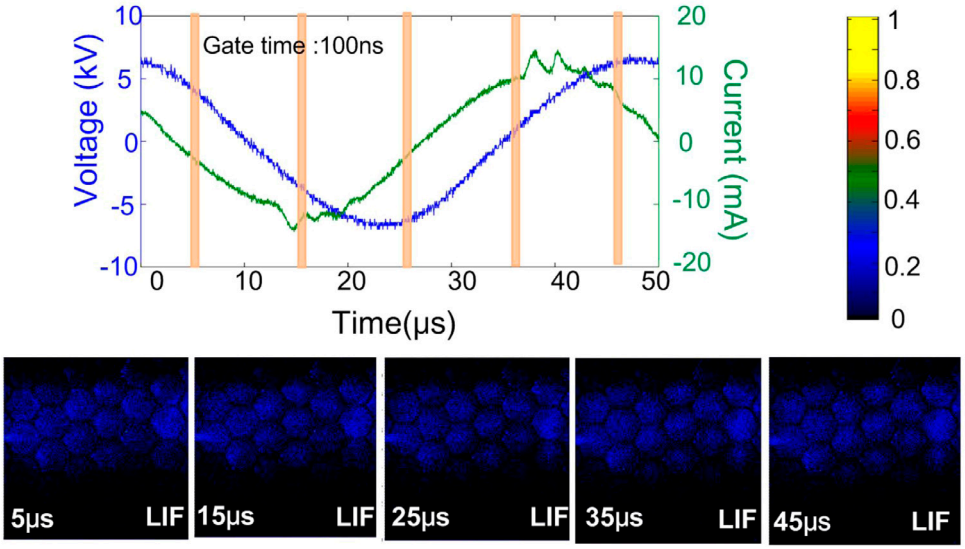

Figure 6. Waveform of the discharge voltage and current (top), LIF images at gate time points of the voltage trace in the mixture of He/0.02%H_2O (bottom).

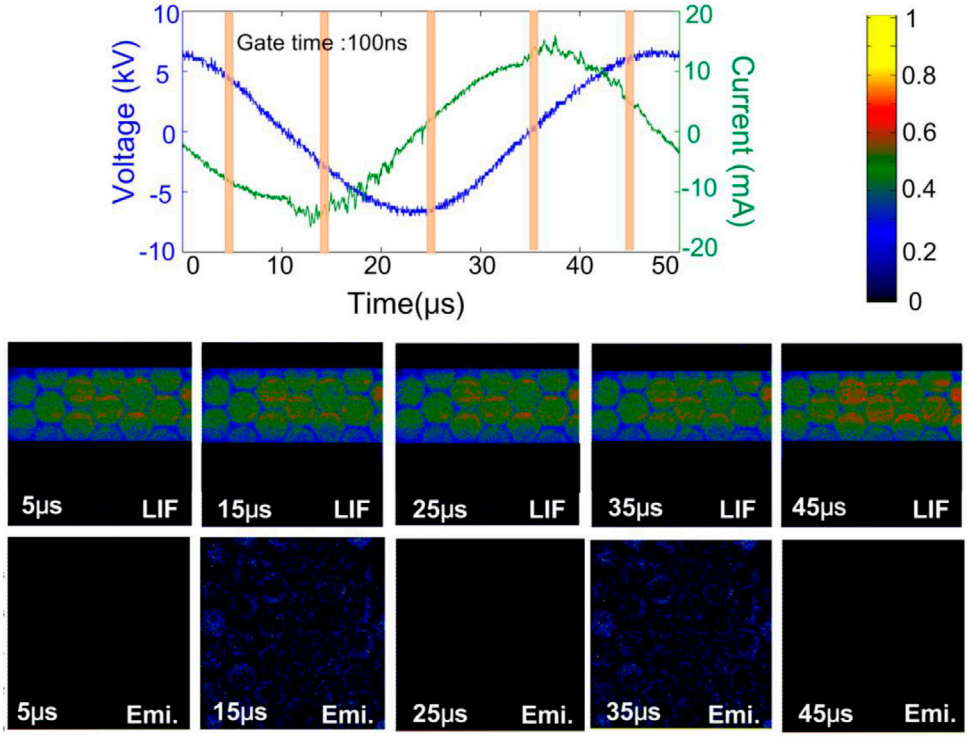

Figure 7. (a) Waveform of the discharge voltage and current; (b) LIF images and 309 nm emission images corresponding to gate time points in the mixture of Ar/0.02%H_2O.

Table 1. Reactions responsible for the loss of OH quoted from the literature.

Reaction	Typical rate ($m^3\ s^{-1}$)	Reference
$OH + OH \rightarrow H_2O + O$	1.9×10^{-18}	[36]
$OH + OH \rightarrow H_2O_2$	2.6×10^{-17}	[37]
$OH + H + He \rightarrow He + H_2O$	1.1×10^{-18}	[35]
$OH + O_2 \rightarrow HO_2 + O$	3.7×10^{-17}	[37]

population. The partial differential equations of population and depopulation processes are as follows [25]:

$$\frac{dN_1}{dt} = L(t)I_s\left(-\frac{B_{12}}{c}f_B^{v''=0,J''=4.5}N_1 + \frac{B_{21}}{c}f_B^{v'=1,J'=3.5}N_2\right) + A_{10}N_2 + (Q_{00} + A_{00})N_3 + V_xN_4 \quad (3.1)$$

$$\frac{dN_2}{dt} = L(t)I_s\left(\frac{B_{12}}{c}f_B^{v''=0,J''=4.5}N_1 - \frac{B_{21}}{c}f_B^{v'=1,J'=3.5}N_2\right) - (Q_{11} + A_{11} + A_{10} + V_A)N_2 \quad (3.2)$$

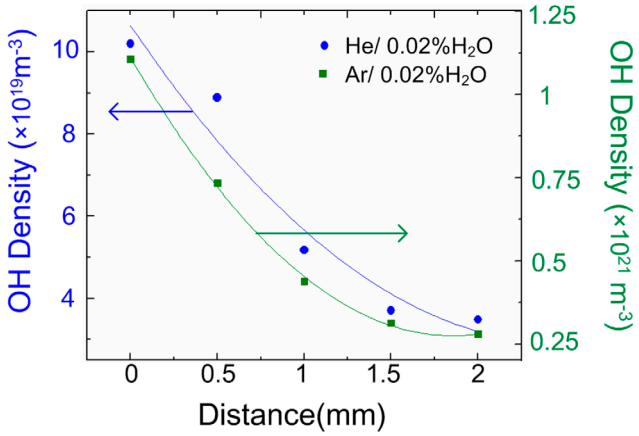

Figure 8. OH density as a function of the distance from the electrode in He/0.02%H_2O and Ar/0.02%H_2O plasma. Results of LIF measurements have a statistical error of about 20%.

$$\frac{dN_3}{dt} = V_A N_2 - (Q_{00} + A_{00})N_3 \tag{3.3}$$

$$\frac{dN_4}{dt} = (A_{11} + Q_{11})N_2 - V_X N_4 \tag{3.4}$$

N_1, N_2, N_3, N_4 are the density in m^{-3} of OH(X, $v'' = 0$), OH(A, $v' = 1$), OH(A, $v' = 1$) and OH(X, $v'' = 1$) states, respectively. $L(t)$ is the normalized function describing the time-resolved behavior of the laser pulse which was measured experimentally. B_{ij} are absorption Einstein coefficients of transition and f Boltzmann factor of the levels with vibrational level v and total angular momentum J. V_A and V_x are the VET rates in the excited and ground state. A_{ij} are emission Einstein coefficients and Q_{ij} are the quenching rate. I_s is the laser spectral irradiance (W m^{-1}) which is determined in according with works [25] as:

$$I_s = \frac{E_{las}\int_{-\infty}^{\infty} Y_A(\nu)L_L(\nu)d\nu}{\Delta\nu_L \tau_L A_L} \tag{3.5}$$

where $\Delta\nu_L$ is the laser width (m^{-1}), A_L is a laser beam area (m^2), τ_L is the laser pulse FWHM (s). In equation (3.5) $Y_A(\nu)$ is the spectral profile of the absorption transition (1 m^{-1}) measured by means of the scanning the laser wavelength around $P_1(4)$ transition and $L_L(\nu)$ is the laser spectral profile (1 m^{-1}) given by the laser specification.

Finally the LIF signal calibrated by the Rayleigh scattering can be presented as:

$$S_{LIF} = \frac{1}{4\pi}\frac{hc}{\lambda}N_{OH}\int(4.29\times10^{12}N_2(t) + 4.69\times10^{12}N_3(t))dt \tag{3.6}$$

where $N_{OH} = n_{exc}/n_{tot}$ is the density of OH radicals in excited state normalized to the total OH density in the ground state. Detailed description of the model, as well as the procedure of LIF signal calibration, is out of the scope of the present work. Required details can be found, together with the data for the modeling, in our previous works [19, 21, 38] as well as in numerous papers focused on OH measurements [26, 25, 39, 40]. The set of equations (3.1)–(3.6) is solved considering

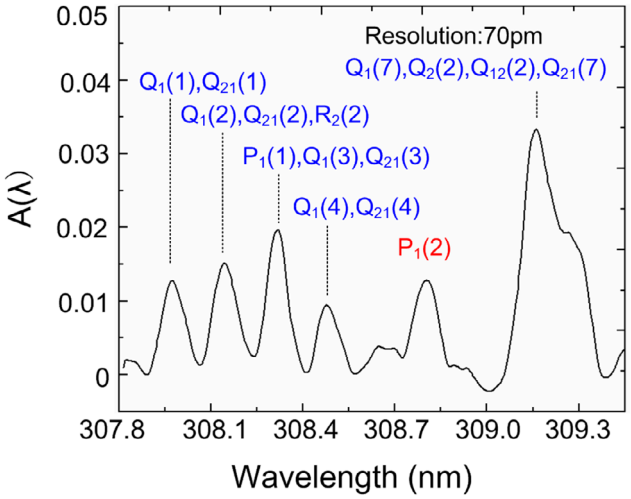

Figure 9. The fractional absorption $A(\lambda)$ obtained in the Ar/0.01%H_2O mixture.

that the density of the quenchers (O_2, N_2, H_2O) depends on the beam position as presented in figure 5. The obtained absolute density of OH radicals in the ground state with increasing the distance in He/0.02%H_2O and Ar/0.02%H_2O plasma is shown in figure 8. The OH density decreases from 1.02×10^{20} m^{-3} at 0 mm to 3.2×10^{19} m^{-3} at 0 mm in He/0.02%H_2O. In the case of Ar/0.02%H_2O, it decays exponentially from 1.12×10^{21} m^{-3} at 0 mm to 2.6×10^{20} m^{-3} at 2 mm away from the electrode.

3.2. UV-BAS of OH radicals

Due to the importance of absolute measurements of OH(X) states, a UV absorption spectroscopy was used. Results of LIF spectroscopy presented in figures 6 and 7 indicate that OH ground state density is almost uniform during one entire voltage period and so a time-integrated OH(X) using UV absorption spectroscopy is a useful measure. The average absolute density of OH(X) radicals in the volume of LED light (light shape is shown in figure 1(a), $z \leqslant 2$ mm) is determined with the broadband absorption in the present work. The output of the UV light source, after passing through the discharge cell, was modulated by a variable light chopper (model 218, Bentham) at 1.5 kHz (figure 1(a)). The lock-in technique provides an advantage of excluding the measurements of plasma radiation and the OH emission generated in the discharge from the absorption experiments. The lock-in amplifier only amplifies the signal at the locking frequency and thus the OH emission generated by the discharge at the frequency of 20 kHz is not amplified and eliminated. At first, the signal from the reference source is detected (I_{off}), when plasma is OFF. Afterwards, the signal (I_{on}) is recorded when the light absorption is taking place by the presence of OH radicals formed in the discharge. The plasma radiation is excluded from the measured signal due to lock-in technique and the fractional absorption of OH(X) is obtained as:

$$A(\lambda) = 1 - \frac{I_{on}}{I_{off}}. \tag{3.7}$$

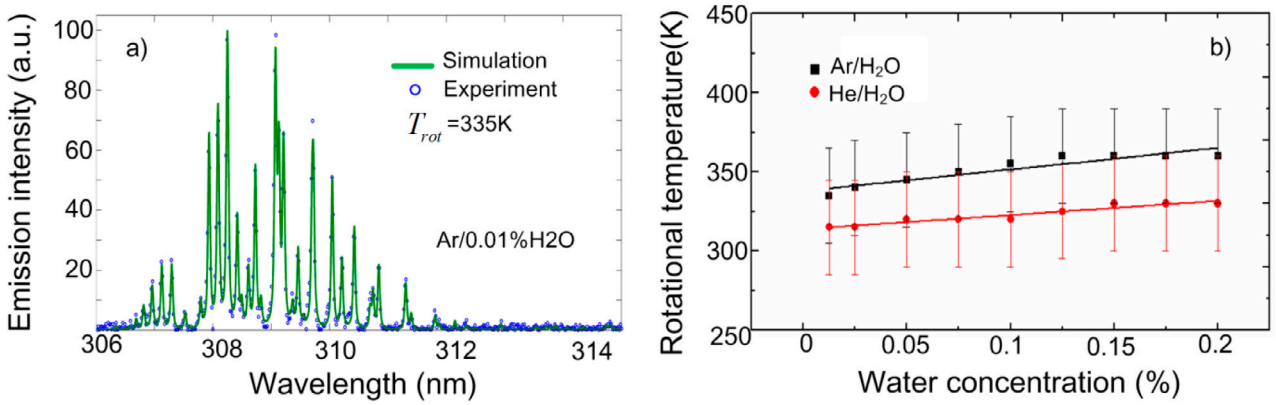

Figure 10. (a) Optical emission spectrum used to determine gas temperature for the Ar/0.01% H_2O plasma; (b) the rotational temperature of the OH molecule as a function of H_2O concentration in both the Ar/H_2O and He/H_2O plasmas.

A typical example of the recorded fractional absorption $A(\lambda)$ is presented in figure 9. The line integrated absorption along the light path of the isolated $P_1(2)$ rational line is chosen for calculation of OH(X) density, and it can be obtained by the Beer–Lambert law [22]:

$$W = \int A(\lambda)\mathrm{d}\lambda = \int 1 - \exp(-h\lambda B_{ij}\phi(\lambda)n_{J''}L)\mathrm{d}\lambda \tag{3.8}$$

where B is the Einstein absorption coefficient, h is the Planck constant, L is the absorption length, $n_{J''}$ is the OH density in a specific level of the ground state, and $\phi(\lambda)$ is the normalized spectral line profile, respectively. The line profile $\phi(\lambda)$ is mainly caused by the Doppler broadening and the van der Walls broadening when the discharge is generated at atmospheric pressure. The Doppler line width is calculated by

$$w_\mathrm{d} = 7.16 \times 10^{-7}\lambda_0\sqrt{\frac{T_\mathrm{g}}{M(\mathrm{OH})}} \tag{3.9}$$

where M(OH) is the molecular weight of OH radical, T_g is the gas temperature and λ_0 is the central wavelength. The van der Waals broadening line width for He is calculated from [22]:

$$w_\mathrm{L} = \frac{\lambda_0^2}{c}1.71 \times 10^{-3}\left(\frac{T_\mathrm{g}}{296}\right). \tag{3.10}$$

The pre-factor for the van der Waals broadening for Ar is taken from [41]. The $\phi(\lambda)$ shape is considered as a Voigt function after convoluting these two broadening mechanisms. It is found that in our system the instrumental broadening dominates other broadening mechanisms for the $P_1(2)$ line and therefore, the measured absorption line is deconvoluted by the instrument function using an algorithm from [42] before the integration of $P_1(2)$ and determination of value W in equation (3.8).

As for the total density of the ground state OH(X), it is given in equation (3.11):

$$n_\mathrm{tot} = n_{J''}/f_{J''} \tag{3.11}$$

$f_{J''}$ is the Boltzmann factor of the rotational level J'', and is given in equation (3.12):

$$f_{J''} = \frac{2J''+1}{2Q_\mathrm{rot}(T_\mathrm{g})}\exp\left(-\frac{E_{J''}}{kT_\mathrm{g}}\right) \tag{3.12}$$

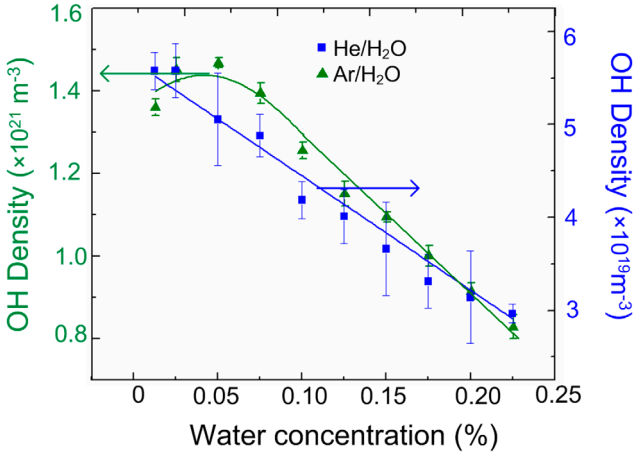

Figure 11. Volume- and time-integrated density of the ground state OH radicals as a function of H_2O content in both the He/H_2O and Ar/H_2O plasmas.

with J'' is the rotational number, $E_{J''}$ is the energy of the rotational level, $Q_\mathrm{rot}(T_\mathrm{g})$ is the rotational partition function. Substitution of equations (3.11) and (3.12) into the right-hand side of equation (3.8) allows estimation of W as a function of the OH(X) density. Therefore, the density of OH(X) for different H_2O concentrations can be obtained by this method if gas temperature is known.

The emission of OH(A–X) band is used to estimate the gas temperature. A high-resolution spectrum was fitted by a simulated one with the gas temperature as a fitting parameter. Figure 10(a) shows, as an example, the fitting of the OH(A–X) spectrum using LIFBASE software [34]. Figure 10(b) shows the rotational temperature OH(A) with increasing the H_2O concentration in both gas mixtures. Despite the simplicity of the emission spectroscopy method, the identification of OH(A) rotational temperature as an indicator of gas temperature can be strongly affected by population processes of OH(A) states. A thorough study of this problem and the drawback of using OH(A) species for gas temperature measurements can be found elsewhere [43–45]. In order to check the validity of the OH(A) temperature estimation we carried out a cross-check of the method by estimation of the rotational temperature from the absorption of OH(X) states as presented in figure 9. In He/H_2O mixture, the OH(X) rotational temperature is about

Table 2. Dominant reactions producing the OH quoted from the literature.

Reaction	Typical rate (m^3 s^{-1})	Remark	Reference
Electron dissociation			
$e^- + H_2O \rightarrow OH + H + e^-$	2.3×10^{-18}–1.8×10^{-16}	T_e = 1–2 eV	[47]
Electron–ion dissociative recombination			
$e^- + H_2O^+ \rightarrow OH + H$	2.6×10^{-14}	T_e = 1 eV	[48]
$e^- + H_3O^+ \rightarrow OH + H_2 + e^-$	10^{-13}	T_e = 1 eV	[49]
Dissociation by radicals and metastables			
$O(^1D) + H_2O \rightarrow OH + OH$	2.2×10^{-16}	$T_g \approx 300$ K	[36]
$O + H_2 \rightarrow OH + H$	9.3×10^{-24}–5.7×10^{-17}	T_g = 300 K–3000 K	[50]
$O + HO_2 \rightarrow OH + O_2$	5.7×10^{-17}	$T_g \approx 300$ K	[51]
$O + H_2O_2 \rightarrow OH + H\,O_2$	1.8×10^{-21}	$T_g \approx 300$ K	[52]
$He^m + H_2O \rightarrow He + OH + H^+ + e$	2.6×10^{-17}	340 K	[30]
Charge exchange			
$Ar^+ + H_2O \rightarrow OH + ArH^+$	0.5×10^{-15}		[53]
$He_2^+ + H_2O \rightarrow OH + HeH^+ + He$	10^{-16}		[54]

Note: T_v: vibrational temperature.

Table 3. Ground state OH(X) density in different plasmas operating in atmospheric pressure.

Discharge	OH density (m^{-3})	Method	Gas	Power	Reference
acDBD	1.7×10^{19}–1.4×10^{20}	LIF, UV abs.	He/H_2O ($\leqslant$3%), (He/Ar)/H_2O ($\leqslant$2.2%) with N_2	37–51 W	[18, 23, 39, 56]
acDBD	5×10^{19}	NIR-CRDS	He/H_2O ($\leqslant$0.67%) with N_2 or O_2	—	[57]
RF glow	4×10^{20}	UV abs.	He/H_2O ($\leqslant$0.11%)	30–130 W	[22]
RF jet	3×10^{19}	LIF	Ar/H_2O ($\leqslant$1%)	10 W	[38]
RF jet	5.4×10^{21}	LIF	Ar	100 W	[58]
μs plasma gun	1×10^{20}	LIF	He	—	[59]
Pulsed streamer discharge	9×10^{20}	LIF	N_2, O_2 with H_2O electrode	—	[60]
Surface pulsed discharge	3×10^{20}	LIF	Ar in liquid interface	—	[61]
RF μ-APPJ	2×10^{20}	CRDS	He/H_2O ($\leqslant$1%)	$<$20 W	[40]
Pulse jet	2.4×10^{19}	LIF	He	$<$10 W	[62]
Pulsed DBD	1.3×10^{21}	LIF	Air	$<$50 W	[63]

330 K $\pm$ 50 K, while it is slightly higher 360 K $\pm$ 50 K in the case of Ar/H_2O mixture. The effect of H_2O admixing in the range 0–0.2% on OH(X) rotational temperature was difficult to measure with absorption spectroscopy, and this is mainly due to the low sensitivity of the method associated with the low resolution of the spectral system. However, good agreement in between both rotational temperatures of OH(A) and OH(X) states obtained by emission spectrum and absorption spectrum clearly indicates the validity of the emission spectroscopy for temperature measurements in our particular case. The obtained results show an increase of the rotational temperature of OH states in both Ar and He with an increase in the humidity of the gas mixture. The fast vibration-to-vibration (V–V) processes and extremely rapid H_2O–H_2O vibrational-to-translation (V–T) process are proposed to be the main reasons for this trend, as indicated in work [46].

The measured value of the fractional absorption has been compared with the value calculated from equation (3.8). Then the total OH(X) density is calculated with equation (3.11). The results for both plasma-forming gases are presented in figure 11.

An increase in the H_2O concentration above 0.05% leads to a decrease in the OH(X) density. In the case of the He/H_2O discharge however, the OH(X) density decreases monotonically with increasing H_2O concentration from about 0.01% to 0.22%. The peak of the OH(X) density may exist below 0.01%, but H_2O concentrations below 0.01% are outside the range of our gas delivery system. It is interesting to note that OH(X) density is 1.45×10^{21} m^{-3} in optimal conditions as measured by the absorption for Ar/0.02% H_2O mixture, and it is only 16% higher than the value obtained by LIF measurement (1.25×10^{21} m^{-3}) for the same mixture nearby the ground electrode as presented in figure 8. In He/0.02% H_2O mixture, the maximum volume-averaged OH(X) density measured by means of absorption is 5.5×10^{19} m^{-3}, while it is about 10×10^{19} m^{-3} in the LIF experiments. Considering that UV absorption gives a volume-averaged value across the light beam, the agreement in between both methods is very good. Higher OH(X) density measured by the absorption in comparison with LIF results can be related to low resolution of absorption measurements of 70 pm that can lead to an overestimation of OH density by equation (3.8).

Remarkably the OH(X) density in the Ar/H_2O discharge is about 25–29 times that in the He/H_2O discharge which is a similar measured difference of OH(A) emission. This difference is much higher than those that have been reported in the DBD [18, 23, 39]. In comparison to most important processes responsible for OH(X) generation, presented in table 2, one expects higher density of hydroxyl radicals in He discharge mainly due to effective charge exchange processes and reaction with He metastables as noted in the literature [55]. However, both LIF and absorption spectroscopy confirm much higher density of OH radicals in the surface barrier discharge though the exact reason of such a difference is still unclear. One of the possible explanations can be related to the facts that a glow-like diffuse plasma is generated in He environment [12] whereas filamentary discharge is observed in Ar. The electron density and electron temperature can be much higher in the core of the filaments that can leads to higher OH(X) and OH(A) production efficiency in the Ar filaments. The OH(X) absolute density measured in the present work is compared to the available literature data in table 3. Since the plasmas under investigation presented in table 3 are different in the input power we indicated the discharge power whenever it was possible to find it in the cited literature.

In atmospheric-pressure DBDs sustained between two parallel-plate electrodes, the OH density obtained by LIF is reported to be about 1.7×10^{19}–1.4×10^{20} m^{-3} in atmospheric-pressure He/H_2O mixture (H_2O content $\leqslant 3\%$) and (He/Ar)/H_2O ($\leqslant 2.2\%$) with admixing of N_2 [18, 23, 39, 56]. Slightly lower OH density has been measured in the effluent of atmospheric-pressure RF plasma jet of about 3×10^{19} m^{-3} in an Ar/H_2O ($\leqslant 1\%$)(10 W) in work [38], while it is about 2.4×10^{19} m^{-3} in pulsed He jet [62] and 2×10^{20} m^{-3} in mixture He/ H_2O ($\leqslant 1\%$) in a device called RF μ-APPJ [40]. At the same time, the OH radical density increases to 5.4×10^{21} m^{-3} when the discharge power is 100 W in Ar plasma jet [58]. The use of a multi-electrode system leads to an increase of the OH density generated by plasma jet [64]. The OH density about 3×10^{20} m^{-3} has been obtained for surface pulsed discharge in the interface between Ar and by Caroline *et al* [61]. For air pulsed DBD [63], the OH radical are mainly produced in the region of tens μm above the dielectric surface, and it is estimated about 1.3×10^{21} m^{-3}. For the biomedical application, it is also important to obtain OH density on the surface of the target. Riès *et al* [59] reported the maximum OH density of 1×10^{20} m^{-3} for a ground metal target.

The OH density of the He/H_2O SMDA measured in this work is 3–6 $\times 10^{19}$ m^{-3}, similar to those mentioned above for other plasma sources. The OH density of the atmospheric-pressure SMDA in the Ar/H_2O mixture, on the other hand, is about 0.9–1.4 $\times 10^{21}$ m^{-3}, and it is significantly higher than the value in the He/H_2O mixture. As suggested above, the higher OH(X) density in the Ar/H_2O mixture may be due to higher electron density and electron temperature in plasma filaments that are more likely to produce in Ar than in He gas. Indeed, the He discharge is generated in a diffuse glow-like mode [12] whereas bright filaments are observed in Ar mixtures that can lead to higher local electron density and temperature in the filaments and corresponding higher production of OH(X) radicals in Ar discharge. For optimization, the OH density can be adjusted by changing the concentration of H_2O and by changing the Ar/He ratio in an Ar/He/H_2O mixture as the plasma-forming gas for atmospheric-pressure SMDA.

4. Conclusions

In this work, the generation of OH radicals and the spatiotemporal dynamics in an atmospheric pressure SMDA are investigated in detail. For this purpose, the broadband UV absorption spectroscopy and the LIF techniques are applied. It is found that OH(A) emission follows the discharge pulse, whereas OH(X) is maintained at the same level during the entire period of the discharge voltage. The H_2O admixture strongly affects the production of OH(X) radicals in the discharge. The H_2O admixture into the Ar gas is found to increase the OH(X) density up to 1.5×10^{21} m^{-3} for Ar/0.05%H_2O at a peak-to-peak voltage of 14 kV. Furthermore an increase of H_2O resulted in a linear decline in the OH(X) density in both gas mixtures. The absolute OH density for Ar/H_2O mixtures is 25–30 times higher than that found in He/H_2O mixtures. Ground state OH(X) radicals are produced across the surface of the ground electrode mainly inside the hexagonal mesh cells and their density decreases rapidly as the detection point moves away from the ground electrode to downstream locations. The rapid OH(X) density decrease in the afterglow implies that a direct effect of the OH radicals on treated materials may become negligibly small at distances more than 5 mm from the grounded electrode. Overall, the results of this work demonstrate that ground state OH radicals are effectively produced in an atmospheric-pressure SMDA along the whole electrode area and the generation of hydroxyl radicals can be controlled by variation of the gas composition through the H_2O vapor admixing. The described plasma source can be used for various applications related to the large-area surface treatment with OH radicals.

Acknowledgments

This work was supported by the National Science Foundation of China (Grant No. 51307134 and 51221005) and China Scholarship Council (CSC). NB acknowledges the support of the ‘Pôle d’Attraction Interuniversitaire’ project (PAI, P7/34, ‘Plasma-surface interaction’), as well as of the ‘REFORGAS GreenWin’ project (grant No. 7267).

References

[1] Laroussi M 2009 Low-temperature plasmas for medicine? *IEEE Trans. Plasma Sci.* **37** 714–25
[2] Kong M G, Kroesen G, Morfill G, Nosenko T, Shimizu T, Van Dijk J and Zimmermann J L 2009 Plasma medicine: an introductory review *New J. Phys.* **11** 115012
[3] Vanraes P *et al* 2015 Decomposition of atrazine traces in water by combination of non-thermal electrical discharge and adsorption on nanofiber membrane *Water Res.* **72** 361–71

[4] Vandamme J, Nikiforov A, Dujardin K, Leys C, De Cooman L and Van Durme J 2015 Critical evaluation of non-thermal plasma as an innovative accelerated lipid oxidation technique in fish oil *Food Res. Int.* **72** 115–25

[5] Penkov O V, Khadem M, Lim W-S and Kim D-E 2015 A review of recent applications of atmospheric pressure plasma jets for materials processing *J. Coat. Technol. Res.* **12** 225–35

[6] Deng X, Nikiforov A Y, De Geyter N, Morent R and Leys C 2013 Deposition of a TMDSO-based film by a non-equilibrium atmospheric pressure DC plasma jet *Plasma Process. Polym.* **10** 641–8

[7] Pons J, Moreau E and Touchard G 2005 Asymmetric surface dielectric barrier discharge in air at atmospheric pressure: electrical properties and induced airflow characteristics *J. Phys. D: Appl. Phys.* **38** 3635–42

[8] Williamson J M, Trump D D, Bletzinger P and Ganguly B N 2006 Comparison of high-voltage ac and pulsed operation of a surface dielectric barrier discharge *J. Phys. D: Appl. Phys.* **39** 4400–6

[9] Morfill G E, Shimizu T, Steffes B and Schmidt H-U 2009 Nosocomial infections—a new approach towards preventive medicine using plasmas *New J. Phys.* **11** 115019

[10] Shimizu T, Sakiyama Y, Graves D B, Zimmermann J L and Morfill G E 2012 The dynamics of ozone generation and mode transition in air surface micro-discharge plasma at atmospheric pressure *New J. Phys.* **14** 103028m

[11] Li D, Liu D, He T, Li Q, Wang X and Kong M G 2015 Three distinct modes in a surface micro-discharge in atmospheric pressure He + N_2 mixtures *Phys. Plasmas* **22** 123501

[12] Li D, Liu D X, Nie Q Y, Li H P, Chen H L and Kong M G 2014 Array of surface-confined glow discharges in atmospheric pressure helium: modes and dynamics *Appl. Phys. Lett.* **104** 204101

[13] Dobrynin D, Friedman G, Fridman A and Starikovskiy A 2011 Inactivation of bacteria using dc corona discharge: role of ions and humidity *New J. Phys.* **13** 103033

[14] Puač N, Miletić M, Mojović M, Popović-bijelić A and Vuković D 2015 Sterilization of bacteria suspensions and identification of radicals deposited during plasma treatment *Open Chem.* **13** 332–8

[15] Stoffels E, Kieft I E and Sladek R E J 2003 Superficial treatment of mammalian cells using plasma needle *J. Phys. D: Appl. Phys.* **36** 2908–13

[16] Van der Paal J, Aernouts S, van Duin A C T, Neyts E C and Bogaerts A 2013 Interaction of O and OH radicals with a simple model system for lipids in the skin barrier: a reactive molecular dynamics investigation for plasma medicine *J. Phys. D: Appl. Phys.* **46** 395201

[17] Dilecce G, Martini L M, Tosi P, Scotoni M and De Benedictis S 2015 Laser induced fluorescence in atmospheric pressure discharges *Plasma Sources Sci. Technol.* **24** 34007

[18] Dilecce G and De Benedictis S 2011 Laser diagnostics of high-pressure discharges: laser induced fluorescence detection of OH in He/Ar–H_2O dielectric barrier discharges *Plasma Phys. Control. Fusion* **53** 124006

[19] Li L, Nikiforov A, Xiong Q, Britun N, Snyders R, Lu X and Leys C 2013 OH radicals distribution in an Ar–H_2O atmospheric plasma jet *Phys. Plasmas* **20** 93502

[20] Wang C and Wu W 2013 Simultaneous measurements of OH(A) and OH(X) radicals in microwave plasma jet-assisted combustion of methane/air mixtures around the lean-burn limit using optical emission spectroscopy and cavity ringdown spectroscopy *J. Phys. D: Appl. Phys.* **46** 464008

[21] Nikiforov A, Li L, Britun N, Snyders R, Vanraes P and Leys C 2014 Influence of air diffusion on the OH radicals and atomic O distribution in an atmospheric Ar (bio) plasma jet *Plasma Sources Sci. Technol.* **23** 15015

[22] Bruggeman P, Cunge G and Sadeghi N 2012 Absolute OH density measurements by broadband UV absorption in diffuse atmospheric-pressure He–H_2O RF glow discharges *Plasma Sources Sci. Technol.* **21** 35019

[23] Dilecce G, Ambrico P F, Simek M and De Benedictis S 2012 OH density measurement by time-resolved broad band absorption spectroscopy in an Ar–H_2O dielectric barrier discharge *J. Phys. D: Appl. Phys.* **45** 125203

[24] Döbele H F, Mosbach T, Niemi K and Der Gathen V S 2005 Laser-induced fluorescence measurements of absolute atomic densities: concepts and limitations *Plasma Sources Sci. Technol.* **14** S31–41

[25] Verreycken T, van der Horst R M, Sadeghi N and Bruggeman P 2013 Absolute calibration of OH density in a nanosecond pulsed plasma filament in atmospheric pressure He–H_2O: comparison of independent calibration methods *J. Phys. D: Appl. Phys.* **46** 464004

[26] Verreycken T, Mensink R, Van Der Horst R, Sadeghi N and Bruggeman P J 2013 Absolute OH density measurements in the effluent of a cold atmospheric-pressure Ar–H_2O RF plasma jet in air *Plasma Sources Sci. Technol.* **22** 55014

[27] Salmon J T and Laurendeau N M 1985 Calibration of laser-saturated fluorescence measurements using Rayleigh scattering *Appl. Opt.* **24** 65–73

[28] Jeon J, Rosentreter T M, Li Y, Isbary G, Thomas H M, Zimmermann J L, Morfill G E and Shimizu T 2014 Bactericidal agents produced by surface micro-discharge (SMD) plasma by controlling gas compositions *Plasma Process. Polym.* **11** 426–36

[29] Paul P H 1994 A model for temperature-dependent collisional quenching of OH $A^2\sum +$ *J. Quant. Spectrosc. Radiat. Transfer* **51** 511–24

[30] Liu D X, Bruggeman P, Iza F, Rong M Z and Kong M G 2010 Global model of low-temperature atmospheric-pressure He + H_2O plasmas *Plasma Sources Sci. Technol.* **19** 25018

[31] Hagelaar G J M and Pitchford L C 2005 Solving the Boltzmann equation to obtain electron transport coefficients and rate coefficients for fluid models *Plasma Sources Sci. Technol.* **14** 722–33

[32] Alves L L *et al* 2013 Comparisons of sets of electron–neutral scattering cross sections and swarm parameters in noble gases: II. Helium and neon *J. Phys. D: Appl. Phys.* **46** 334002

[33] Tamura M, Berg P A, Harrington J E, Luque J, Jeffries J B, Smith G P and Crosley D R 1998 Collisional quenching of CH(A), OH(A), and NO(A) in low pressure hydrocarbon flames *Combust. Flame* **114** 502–14

[34] Luque J and Crosley D R 1999 Lifbase: database and spectral simulation program (version 1.5) *SRI International Report* MP 99(009)

[35] Kienle R, Lee M P and Kohse-Höinghaus K 1996 A detailed rate equation model for the simulation of energy transfer in OH laser-induced fluorescence *Appl. Phys.* B **62** 583–99

[36] Herron J T and Green D S 2001 Chemical kinetics database and predictive schemes for nonthermal humid air plasma chemistry. Part II. Neutral species reactions *Plasma Chem. Plasma Process.* **21** 459–81

[37] NIST 2015 Chemical kinetics database standard reference database 17, version 7.0 (web version), release 1.6.8 (http://kinetics.nist.gov/kinetics/index.jsp)

[38] Xiong Q, Nikiforov A Y, Li L, Vanraes P, Britun N, Snyders R, Lu X P and Leys C 2012 Absolute OH density determination by laser induced fluorescence spectroscopy in an atmospheric pressure RF plasma jet *Eur. Phys. J.* D **66** 281

[39] Dilecce G, Ambrico P F, Simek M and De Benedictis S 2012 LIF diagnostics of hydroxyl radical in atmospheric

pressure He–H_2O dielectric barrier discharges *Chem. Phys.* **398** 142–7
[40] Benedikt J, Schröder D, Schneider S, Willems G, Pajdarová A, Vlček J and Schulz-von der Gathen V 2016 Absolute OH and O radical densities in effluent of a He/H_2 O micro-scaled atmospheric pressure plasma jet *Plasma Sources Sci. Technol.* **25** 45013
[41] Kasyutich V L 2005 Pressure broadening parameters of the hydroxyl radical $A^2\Sigma + (\upsilon = 0) \leftarrow X^2\Pi$ 3/2 $(\upsilon = 0)$ transitions at ca. 308 nm *Eur. Phys. J.* D **33** 29–33
[42] Petrov G M 2002 A simple algorithm for spectral line deconvolution *J. Quant. Spectrosc. Radiat. Transfer* **72** 281–7
[43] Pichamuthu J P 1972 Gas-temperature measurement in pulsed H_2O laser discharges *J. Appl. Phys.* **43** 4562
[44] Bruggeman P, Schram D, González M A, Rego R, Kong M G and Leys C 2009 Characterization of a direct dc-excited discharge in water by optical emission spectroscopy *Plasma Sources Sci. Technol.* **18** 25017–13
[45] Bruggeman P, Verreycken T, González M Á, Walsh J L, Kong M G, Leys C and Schram D C 2010 Optical emission spectroscopy as a diagnostic for plasmas in liquids: opportunities and pitfalls *J. Phys. D: Appl. Phys.* **43** 124005
[46] Ono R, Nakagawa Y and Oda T 2011 Effect of pulse width on the production of radicals and excited species in a pulsed positive corona discharge *J. Phys. D: Appl. Phys.* **44** 485201
[47] Itikawa Y and Mason N 2005 Cross sections for electron collisions with water molecules *J. Phys. Chem. Ref. Data* **34** 1
[48] Nakagawa Y, Ono R and Oda T 2011 Density and temperature measurement of OH radicals in atmospheric-pressure pulsed corona discharge in humid air *J. Appl. Phys.* **110** 73304
[49] Millar T J, Farquhar P R A and Willacy K 1997 The UMIST database for astrochemistry 1995 *Ser. Astron. Astrophys. Suppl. Ser.* **139** 139–85
[50] Baulch D L *et al* 1994 Summary table of evaluated kinetic data for combustion modeling: supplement 1 *Combust. Flame* **98** 59–79
[51] Tsang W and Hampson R F 1986 Chemical kinetic data base for combustion chemistry. Part I. Methane and related compounds *J. Phys. Chem. Ref. Data* **15** 1087
[52] Atkinson R, Baulch D L, Cox R A, Hampson R F, Kerr J A, Rossi M J and Troe J 1997 Evaluated kinetic and photochemical data for atmospheric chemistry: supplement VI. IUPAC subcommittee on gas kinetic data evaluation for atmospheric chemistry *J. Phys. Chem. Ref. Data* **26** 1329
[53] Ikezoe Y, Matsuoka S, Takebe M and Viggiano A1988 Gas phase ion—molecule reaction rate constants through 1986 *Int. J. Mass Spectrom. Ion Process.* **84** R17–8
[54] Massines F, Sarra-Bournet C, Fanelli F, Naudé N and Gherardi N 2012 Atmospheric pressure low temperature direct plasma technology: status and challenges for thin film deposition *Plasma Process. Polym.* **9** 1041–73
[55] Bruggeman P and Schram D C 2010 On OH production in water containing atmospheric pressure plasmas *Plasma Sources Sci. Technol.* **19** 45025
[56] Martini L M, Dilecce G, Scotoni M, Tosi P and De Benedictis S 2014 OH density measurements by time-resolved broad band absorption spectroscopy in a He–H_2O dielectric barrier discharge with small O_2 addition *Plasma Process. Polym.* **11** 232–8
[57] Liu Z W, Yang X F, Zhu A M, Zhao G L and Xu Y 2008 Determination of the OH radical in atmospheric pressure dielectric barrier discharge plasmas using near infrared cavity ring-down spectroscopy *Eur. Phys. J.* D **48** 365–73
[58] Voráč J, Obrusník A, Procházka V, Dvořák P and Talába M 2014 Spatially resolved measurement of hydroxyl radical (OH) concentration in an argon RF plasma jet by planar laser-induced fluorescence *Plasma Sources Sci. Technol.* **23** 25011
[59] Riès D, Dilecce G, Robert E, Ambrico P F, Dozias S and Pouvesle J-M 2014 LIF and fast imaging plasma jet characterization relevant for NTP biomedical applications *J. Phys. D: Appl. Phys.* **47** 275401
[60] Yagi I, Shirakawa Y, Hirakata K, Akiyama T, Yonemori S, Mizuno K, Ono R and Oda T 2015 Measurement of OH, O, and NO densities and their correlations with mouse melanoma cell death rate treated by a nanosecond pulsed streamer discharge *J. Phys. D: Appl. Phys.* **48** 424006
[61] Winters C, Petrishchev V, Yin Z, Leonov S B, Lempert W R, Adamovich I V, Chaszeyka M A, Thermodynamics N and Zentrum D 2015 Surface charge dynamics and OH and H number density distributions in near-surface nanosecond pulse discharges at a liquid/vapor interface *J. Phys. D: Appl. Phys.* **48** 424002
[62] Pei X, Wu S, Xian Y, Lu X and Pan Y 2014 On OH density of an atmospheric pressure plasma jet by laser-induced fluorescence *IEEE Trans. Plasma Sci.* **42** 1206–10
[63] Teramoto Y, Kim H-H, Ogata A and Negishi N 2014 Measurement of OH ($X^2\Sigma$) in immediate vicinity of dielectric surface under pulsed dielectric barrier discharge at atmospheric pressure using two geometries of laser-induced fluorescence *J. Appl. Phys.* **115** 133302
[64] Yue Y, Pei X and Lu X 2016 OH density optimization in atmospheric-pressure plasma jet by using multiple ring electrodes *J. Appl. Phys.* **119** 33301